Matrix Methods for the Dynamic Range Optimization of Continuous-Time G_m-C Filters

Juan F. Fernández-Bootello, Manuel Delgado-Restituto, *Member, IEEE*, and Angel Rodríguez-Vázquez, *Fellow, IEEE*

***Abstract*—This paper presents a synthesis procedure for the optimization of the dynamic range of continuous-time fully differential G_m-C filters. Such procedure builds up on a general extended state-space system representation which provides simple matrix algebra mechanisms to evaluate the noise and distortion performances of filters, as well as, the effect of amplitude and impedance scaling operations. Using these methods, an analytical technique for the dynamic range optimization of weakly nonlinear G_m-C filters under power dissipation constraints is presented. The procedure is first explained for general filter structures and then illustrated with a simple biquadratic section.**

***Index Terms*—G_m-C filters, filter synthesis, dynamic range optimization, noise analysis, distortion analysis, low power.**

I. Introduction

FULLY DIFFERENTIAL G_m-C circuits and techniques are widely employed to design integrated continuous-time filters. Over the years significant contributions have been made regarding the proposal of transconductor topologies with enhanced *noise* and *distortion* performance. Based on such transconductors, filters with enlarged *dynamic range (DR)*[1] can be built for different practical applications. However, despite the availability of high-performance transconductors, dynamic range optimization may be hampered due to inaccurate evaluation of the impact of noise and distortion on the overall filter performance.

Regarding the impact of noise, one of the most significant early contributions was due to Groenewold [1]. He employed *state-space* descriptions to evaluate noise performance through simple *matrix manipulations*. Similar approaches to noise evaluation have been used in [2], [3]. In this paper, we adopt these noise evaluation techniques. Also, we adopt the *general* G_m-C structure proposed in [3].

Regarding the impact of distortion, different techniques have been reported; for instance, those presented in [4]–[9]. Proposals in [4], [5] are based on frequency-domain calculation using Volterra series which, although powerful, tend to be very cumbersome as the filter order increases. In [6], [7] nonlinearities of individual transconductors are propagated by means of partial transfer functions to the output, where the contributions are summed to estimate the overall distortion behavior of the filter. Finally, [8], [9] use time-domain analysis and state-space modelling for the evaluation of harmonic and intermodulation distortion in filters with no floating capacitors. None of these approaches provides the *simple, general and systematic* matrix manipulation techniques which are available for noise. Consequently, no systematic method is yet available to evaluate the impact of both noise and distortion on a general G_m-C filter structure, thereby limiting the ability of designers to maximize the dynamic range of practical filter implementations.

This paper presents methods and techniques to evaluate the impact of both noise and distortion on the G_m-C filter structure of [3] through simple and systematic matrix algebra. For distortion evaluation we combine state-space and Volterra Series representations [10] in such a way that they can be easily embedded in matrix form.

The paper also addresses the issue of *scaling*. The optimization of *DR* through modifications of the amplitude and impedance levels at the internal filter nodes is covered for both *biquadratic sections* and *general* G_m-C filters. In the case of biquadratic sections, the paper reports compact *DR* expressions which provide more accurate estimations of the influence of the quality factor, Q, than those in [1]. For general filters, the techniques presented in this paper overcome the lack of univocal solutions observed in the approach presented in [6].

The paper is structured as follows. Section II describes the state-space representation of general G_m-C filters, and provides relationships among the state-space matrix and a set of internal transfer functions which are essential for the foregoing analysis. Sections III and IV present the systematic techniques for the evaluation of noise and distortion, respectively. Section V deals with the scaling of G_m-C filters. Section VI addresses the dynamic range optimization of generic G_m-C filters and the procedure is illustrated in Section VII for biquad structures. Finally, Section VIII concludes the paper.

Manuscript received October 22, 2007; revised January 11, 2008. First published April 18, 2008; current version published October 29, 2008. This work was supported by the Spanish Ministry of Education & Science under Grant TEC2006-03022, and the Junta de Andalucía under Grant TIC-02818. This paper was recommended by Associate Editor T. B. Tarim.

J. F. Fernández-Bootello and A. Rodríguez-Vázquez are with AnaFocus, Sevilla 41092, Spain.

M. Delgado-Restituto is with the Instituto de MicroelectrÓnica de Sevilla, Centro Nacional de Microelectrónica, Consejo Superior de Investigaciones Científicas (CSIC), and Universidad de Sevilla, 41012 Sevilla, Spain (e-mail: Manuel.Delgado@imse.cnm.es).

Digital Object Identifier 10.1109/TCSI.2008.921048

[1]*DR* is defined as the ratio between the maximum and minimum signal that can be processed by the filter. The latter is limited by the total integrated output-referred noise power of the filter, $\overline{U_{no}^2}$, and the former is limited by the maximum output distortion level which can be tolerated. Assuming a single-tone excitation and letting be the maximum signal level at the output of the filter, the dynamic range can be expressed as

$$DR = (1/2) \cdot (\rho_{max}^2/\overline{U_{no}^2}) \equiv P_{max}/\overline{U_{no}^2}$$

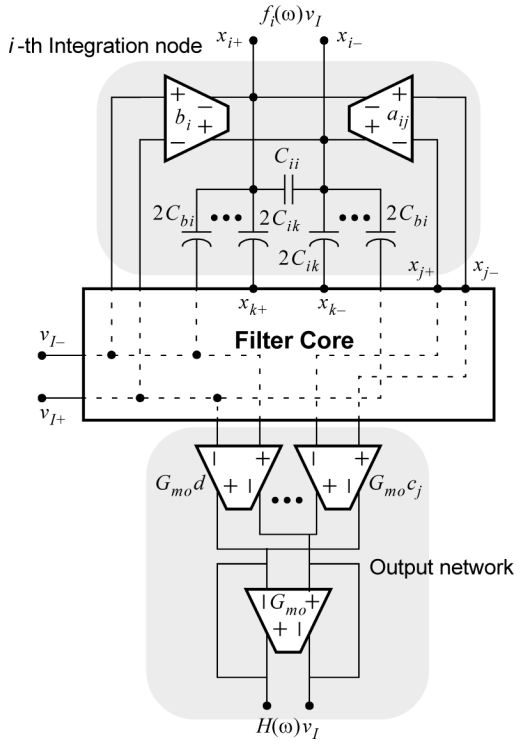

Fig. 1. Simplified schematic of a fully balanced G_m-C filter.

II. Space-State Representation of G_m-C Filters

Fig. 1 shows the conceptual schematic of a generic continuous-time fully balanced G_m-C filter with n integration nodes. We assume that each integration node can be connected to the input and to all the remaining integration nodes; we further assume that these connections can be realized with either capacitors or transconductors. It is illustrated in Fig. 1 for a generic integration node $x_i = x_{i+} - x_{i-}$, $i = 1, \ldots, n$. Capacitive connections to other integration nodes are realized with capacitors C_{ik}, $k = 1, \ldots, n$; transconductance connections to other integration nodes are realized with transconductors a_{ij}, $j = 1, \ldots, n$; connections to the input are realized with capacitors C_{bi} and transconductors b_i, respectively. This general diagram contemplates also the general case where the filter output is obtained as the linear combination of the input and an arbitrary number of internal node voltages. Using an extended state-space notation, the filter is described as [3]

$$\begin{aligned} s\mathbf{E}\mathbf{x} &= \mathbf{A}\mathbf{x} + \mathbf{B}v_I \\ v_O &= \mathbf{C}\mathbf{x} + dv_I \end{aligned} \tag{1}$$

which is actually a generalization of the representation given in [1]. In the expression above:

- v_I and v_O are, respectively, the input and output voltages of the filter and $\mathbf{x} = [x_1, x_2, \ldots, x_n]^{\mathrm{T}}$ is a state vector which gathers all the n integration node voltages. Operator $(\cdot)^{\mathrm{T}}$ denotes matrix transpose.
- $\mathbf{A}$ is an $n \times n$ matrix whose element a_{ij} represents the transconductance of the transconductor connected from node x_j to node x_i.
- $\mathbf{B}$ is an $n \times 1$ vector given by

$$\begin{aligned} \mathbf{B} &= \mathbf{B}_G + s\mathbf{B}_C \\ &= [b_1 + sC_{b1}, \ldots, b_n + sC_{bn}]^{\mathrm{T}} \end{aligned} \tag{2}$$

  where b_i and C_{bi} represent, respectively, the transconductance and capacitance between the filter input node and the integration node x_i; $\mathbf{B}_G$ is formed by transconductances and $\mathbf{B}_C$ is composed by capacitances.
- $\mathbf{C}$ in (1) is a $1 \times n$ vector whose element c_j denotes the voltage amplification between node x_j and the output; realized by a transconductor with input x_j and transconductance $G_{mo}c_j$, loaded with a resistor of resistance $1/G_{mo}$ implemented by a feedback transconductor [see Fig. 1(a)]. Parameter d is the voltage gain of the forward path from the input to the output of the filter; realized by a transconductor with gain $G_{mo}d$ loaded by the same feedback transconductor as before.[2]
- Finally, $\mathbf{E}$ is an $n \times n$ matrix composed by capacitances with the following structure:

$$\mathbf{E} = \begin{vmatrix} C_{b1} + \sum_k C_{1k} & -C_{12} & \cdots & -C_{1n} \\ -C_{21} & C_{b2} + \sum_k C_{2k} & \cdots & -C_{2n} \\ \cdots & \cdots & \cdots & \cdots \\ -C_{n1} & -C_{n2} & \cdots & C_{bn} + \sum_k C_{nk} \end{vmatrix} \tag{3}$$

  where the negative and positive components of the integration nodes are chosen such that all the out-of-diagonal entries are negative.

In conventional G_m-C structures, the anti-diagonal entries of $\mathbf{E}$, namely e_{ij} and e_{ji}, coincide as they represent the same capacitor. However, there are practical topologies which lead to non-symmetrical $\mathbf{E}$ matrices. This happens, for instance, in the so-called G_m-C opamp structures where the integrating capacitor is connected in feedback configuration around one opamp [11].

From the representation in (1) the input–output transfer function of the filter can be calculated as

$$H(s) = \frac{v_O}{v_I} = \mathbf{C}(s\mathbf{E} - \mathbf{A})^{-1}\mathbf{B} + d \tag{4}$$

In addition to this overall transfer function, other functions need to be defined. On the one hand, let f_i be the transfer function from v_I to the integration node x_i. It can be shown that

$$\mathbf{F} = (s\mathbf{E} - \mathbf{A})^{-1}\mathbf{B} \tag{5}$$

where

$$\mathbf{F} = [f_1, f_2, \ldots, f_n]^{\mathrm{T}} \tag{6}$$

[2]For the sake of generality the mathematical formulation in the paper considers the general representation above. In many practical situations, there is no forward path from the input so that $d = 0$. Also, in many cases the output of the filter is taken from a single internal node so that only one entry of vector C is non-zero (i.e., $\mathbf{C} = [0, \ldots, c_j, \ldots, 0]$). Moreover, if no output voltage amplification is required, then vector $\mathbf{C}$ is unitary (the only non-zero entry has unity value) and the output summing network can be suppressed.

On the other hand, let g_i be the transfer function from a current source connected to integration node x_i (between the output terminals of transconductors with gain a_{ij} for $j = 1, \ldots, n$) to the filter output for $v_I = 0$. If all the transfer functions g_i, $i = 1, \ldots, n$, are collected into a vector

$$\mathbf{G} = [g_1, g_2, \ldots, g_n] \tag{7}$$

it is easy to show that

$$\mathbf{G} = \mathbf{C}(s\mathbf{E} - \mathbf{A})^{-1}. \tag{8}$$

As will be shown afterwards, vectors F and G significantly simplify the evaluation of filter distortion. Also, they are useful to calculate the relative sensitivities of the filter transfer function $H(s)$ with respect to the matrices in the representation (1). They can be easily obtained using the Hadamard product as[3]

$$\begin{aligned} S|_{\mathbf{A}}^{H(s)} &= \frac{(\mathbf{FG})^{\mathrm{T}} \bullet \mathbf{A}}{H(s)} \\ S|_{\mathbf{E}}^{H(s)} &= \frac{s(\mathbf{FG})^{\mathrm{T}} \bullet \mathbf{E}}{H(s)} \\ S|_{\mathbf{B}}^{H(s)} &= \frac{\mathbf{G}^{\mathrm{T}} \bullet \mathbf{B}}{H(s)} \\ S|_{\mathbf{C}}^{H(s)} &= \frac{\mathbf{F}^{\mathrm{T}} \bullet \mathbf{C}}{H(s)} \\ S|_{d}^{H(s)} &= \frac{d}{H(s)} \end{aligned} \tag{9}$$

where the sensitivities are defined as $S|_x^y = (\partial y/\partial x) \cdot (x/y)$.

Up to now, it has been assumed that transconductances remain constant with frequency. In a more general case, the representation in (1) must be extended to also cope with frequency-dependent transconductances [7]. This can be done at the price of a more complex state-space matrix description. As an example, let us assume that transconductance a_{ij} exhibits a one-pole roll-off with time constant τ_l. This can be modelled by replacing transconductor a_{ij} by the network at the right of Fig. 2(a), where $\tau_l = C_{pl}/G_{ml}$ and the low-frequency transconductance is given by a_{lj}.

Note that this model adds a new node to the topology (labelled l) per transconductor. Hence, matrices of the extended state-space representation must be rebuilt. This is indicated in Fig. 2(b) which shows the rows and columns that must be added to account for the new filter node, l. For consistency, the low frequency behavior a_{lj} must be made equal to the original frequency-independent entry a_{ij} in (1).

III. Noise in G_m-C Filters

We assume noise is only contributed by transconductors and that frequency is high enough so that noise behavior is dominated by thermal contributions. Thermal noise contributions from different transconductors are assumed un-correlated (this is supported by the fact that transconductors are different physical entities), and are modelled by output current noise sources with double-sided *power spectral density (PSD)* $2kT\xi G_m$ where G_m is the transconductance, k is Boltzmann's constant,

[3]The Hadamard product of two $m \times n$ matrices A and B, denoted by $\mathbf{A} \bullet \mathbf{B}$, is an $m \times n$ matrix given by $(\mathbf{A} \bullet \mathbf{B})_{ij} = a_{ij} b_{ij}$ [4].

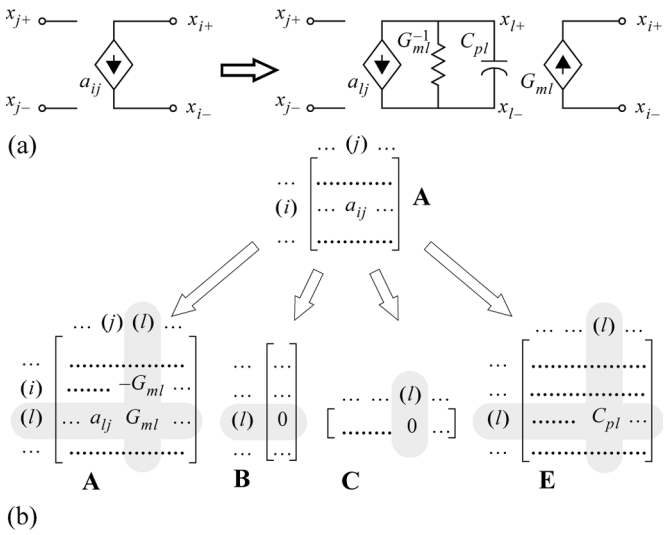

Fig. 2. (a) Circuit replacement for adding one-pole roll-off transconductance characteristics to the generic schematic of Fig. 1(a). (b) Required modifications on the state-space matrices.

T is the absolute temperature and ξ is the noise excess factor of the transconductor—the value of this latter parameter depends on the actual transconductor implementation [12].

Using the transfer functions g_i defined in the previous section [see (7) and (8)], the total output-referred noise voltage *PSD* of the filter can be expressed as

$$S_G(\omega) = 2kT\xi \sum_i |g_i(\omega)|^2 (|b_i| + \sum_j |a_{ij}|) + \frac{2kT\xi}{G_{mo}} (|d| + \sum_i |c_i|). \tag{10}$$

Here, the first term accounts for the noise contributions of all transconductors in the filter core. The second term corresponds to the output summing structure. From now on we will assume that this second term is either negligible (which occurs for large enough values of G_{mo} as it happens in practice), or null (which corresponds to the case where the filter output is simply taken from a single internal node). With this assumption, the total output noise of the filter is approximately given by

$$\overline{U_{no}^2} \approx \frac{kT\xi}{\pi} \int_{-\infty}^{\infty} \sum_i |g_i(\omega)|^2 \left(|b_i| + \sum_j |a_{ij}| \right) d\omega \tag{11}$$

which represents an upper-limit value.

In order to evaluate the integral in (11) it is worth noting that matrix $\mathbf{W}$, defined as [1], [13][4]

$$\tilde{w} = \frac{1}{2\pi} \int_{-\infty}^{+\infty} \mathbf{G}^{\mathrm{T}}(-j\omega) \mathbf{G}(j\omega) d\omega \tag{12}$$

can be algebraically obtained from the following generalized Lyapunov equation [14]:

$$\mathbf{E}^{\mathrm{T}} \mathbf{W} \mathbf{A} + \mathbf{A}^{\mathrm{T}} \mathbf{W} \mathbf{E} = -\mathbf{C}^{\mathrm{T}} \mathbf{C} \tag{13}$$

[4]$\mathbf{W}$ is related to the observability grammian of the system, $\mathbf{W_o}$, as $\mathbf{W_o} = \mathbf{E}^{\mathrm{T}} \mathbf{W} \mathbf{E}$ [15].

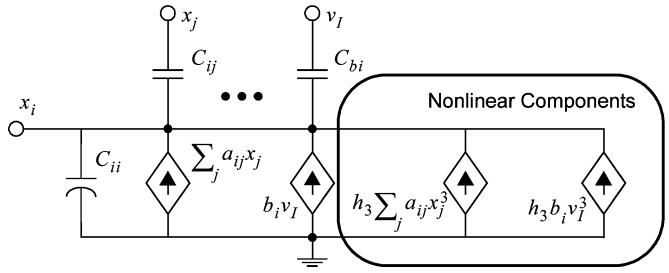

Fig. 3. Conceptual schematic at the ith integration node of the filter including nonlinearities.

and, therefore, the total noise of the filter can be written as

$$\overline{U_{no}^2} = \sum_i 2kT\xi w_{ii} G_{mi} \equiv \sum_i \overline{U_{no,i}^2} \tag{14}$$

where $w_{ii},\ i = 1,\ldots,n$, represent the elements at the diagonal of matrix $\mathbf{W}, G_{mi} = |b_i| + \sum_j |a_{ij}|$ is the sum of all the transconductances driving node i. In the right-hand side of this equation, $\overline{U_{no,i}^2}$ represents the noise contributed to the output from the ith integration node.

IV. Distortion in G_m-C Filters

We focus here on the impact of nonlinearities on the input–output voltage-to-current transformation. Assuming weakly nonlinear operation conditions and that transconductors are fully balanced; their input–output characteristic can be approximated by

$$i \approx G_m v(1 + h_3 v^2) \tag{15}$$

where h_3 is the third-order nonlinearity coefficient and v is the input voltage. This simplified model, where even-order nonlinear coefficients are null because of the balanced structure, suffices for most practical transconductors [11], [12].

Let us first consider that the output summing structure of Fig. 1(a) does not generate distortion; the influence of this structure will be computed in later on. Using (15), the extended state-space representation in (1) becomes

$$\begin{aligned} \mathbf{E}\frac{d\mathbf{x}}{dt} - \mathbf{B}_C\frac{dv_I}{dt} &= \mathbf{A}\mathbf{x} + h_3\mathbf{A}\mathbf{x}^{(3)} + \mathbf{B}_G v_I + h_3\mathbf{B}_G v_I^3 \\ v_O &= \mathbf{C}\mathbf{x} + dv_I \end{aligned} \tag{16}$$

where $\mathbf{x}^{(3)} = [x_1^3, x_2^3, \ldots, x_n^3]^{\mathrm{T}}$ is the Hadamard cube of $\mathbf{x}$ (it is obtained by three consecutive Hadamard products—see footnote 3). For illustration purposes, Fig. 3 shows a conceptual schematic (single-ended for simplicity of the drawing) which displays the components which contribute to the ith integration node according to (16). In this figure, the linear and nonlinear components are clearly separated.

Several approaches are found in literature for the analysis of the nonlinear behavior described by (16), [4]–[9]. Here we use Volterra's series expansions [10]. This method consists in decomposing the internal nodes variables in operators, according to [16]

$$\mathbf{x}(\alpha v_I(t)) = \sum_k \alpha^k \mathbf{x}_k(v_I(t)) \tag{17}$$

where $v_I(t)$ is the input signal of the system, α is an arbitrary amplitude scaling factor

$$\begin{aligned} \mathbf{x}_k(v_I(t)) = \int_{-\infty}^{+\infty} \cdots \int_{-\infty}^{+\infty} \mathbf{h}_k(\tau_1 \ldots \tau_k) \\ \times v_I(t-\tau_1)\ldots v_I(t-\tau_k) d\tau_1 \ldots d\tau_k \end{aligned} \tag{18}$$

is referred to as the kth order Volterra operator and $\mathbf{h}_k(\cdot)$ is the kth Volterra kernel [10]. The Laplace transform of this multidimensional kernel is defined as

$$\begin{aligned} \mathbf{H}_k(s_1,\ldots,s_k) = \int_{-\infty}^{+\infty} \cdots \int_{-\infty}^{+\infty} \mathbf{h}_k(\tau_1 \ldots \tau_k) \\ \times e^{-(s_1\tau_1 \ldots + s_k\tau_k)} d\tau_1 \ldots d\tau_k \end{aligned} \tag{19}$$

where s_k is the k-dimensional Laplace variable. Function $\mathbf{H}_k(s_1,\ldots,s_k)$ describes in frequency-domain the kth order distortion performance of the system. Hence, $\mathbf{H}_1(s_1)$ describes the linear behavior of the system, $\mathbf{H}_3(s_1,s_2,s_3)$ accounts for the third-order nonlinear behavior, and so on.

The relevant feature of Volterra's series expansions approach is that, for weakly nonlinear systems and low values of α, series (17) rapidly converges and it can be approximated by the first few terms. Therefore, if the distortion behavior of a fully balanced G_m-C filter is dominated by the third-order nonlinearities of the transconductors, $\mathbf{x}(\alpha v_I)$ can be simply approximated by $\mathbf{x}(\alpha v_I) \approx \alpha\mathbf{x}_1(v_I) + \alpha^3\mathbf{x}_3(v_I)$. Replacing this expression in (16) and grouping terms with the same power of α, the following two linear systems in $\mathbf{x}_1$ and $\mathbf{x}_3$ are obtained

$$\begin{aligned} \mathbf{E}\frac{d}{dt}\mathbf{x}_1 - \mathbf{B}_C\frac{dv_I}{dt} &= \mathbf{A}\mathbf{x}_1 + \mathbf{B}_G v_I \\ v_{O1} &= \mathbf{C}\mathbf{x}_1 + dv_I \end{aligned} \tag{20}$$

and

$$\begin{aligned} \mathbf{E}\frac{d}{dt}\mathbf{x}_3 &= \mathbf{A}\mathbf{x}_3 + h_3\left(\mathbf{A}\mathbf{x}_1^3 + \mathbf{B}_G v_I^3\right) \\ v_{O3} &= \mathbf{C}\mathbf{x}_3 \end{aligned} \tag{21}$$

where $v_O = v_{O1} + v_{O3}$. The first equations of these two systems can be mapped into the first- and third-order circuits shown in Fig. 4(a) and (b), respectively. Solving both circuits, the first- and third-order transformed kernels of the filter are respectively given by

$$\mathbf{H}_1(s_1) = \mathbf{x}_1/v_I = (\mathbf{E}s_1 - \mathbf{A})^{-1}\mathbf{B} \tag{22}$$

and

$$\begin{aligned} \mathbf{H}_3(s_1,s_2,s_3) &= \mathbf{x}_3/v_I \\ &= h_3(\mathbf{E}(s_1+s_2+s_3) - \mathbf{A})^{-1} \\ &\quad \times (\mathbf{A}(\mathbf{H}_1(s_1) \bullet \mathbf{H}_1(s_2) \bullet \mathbf{H}_1(s_3)) + \mathbf{B}_G) \end{aligned} \tag{23}$$

From these expressions, the third-order harmonic distortion of the filter and its intermodulation performance can be estimated, with no transient analysis needed, by [16]

$$\begin{aligned} HD_3(\omega) &= \frac{1}{4}\left|\frac{\mathbf{C}\mathbf{H}_3(j\omega,j\omega,j\omega)}{\mathbf{C}\mathbf{H}_1(j\omega)}\right|\rho^2 \\ IM_3(2\omega_1 \pm \omega_2) &= \frac{3}{4}\left|\frac{\mathbf{C}\mathbf{H}_3(j\omega_1,j\omega_1,\pm j\omega_2)}{\mathbf{C}\mathbf{H}_1(j\omega_1)}\right|\rho^2 \end{aligned} \tag{24}$$

where ρ is the amplitude of the input tones applied to the system.

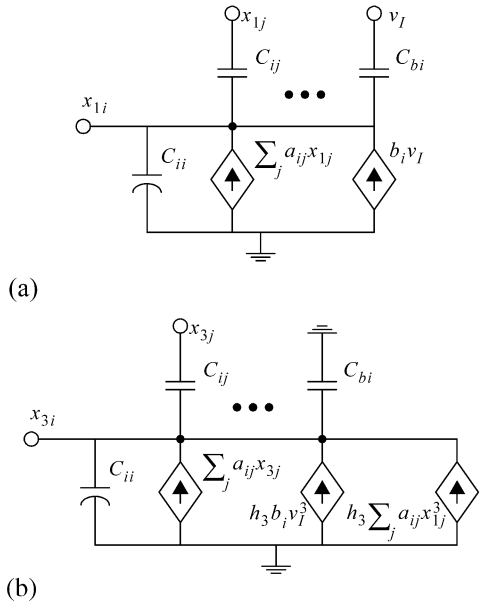

Fig. 4. (a) First-order and (b) third-order circuits at node i.

Equation (24) can be related to vectors $\mathbf{F}$ and $\mathbf{G}$, defined in (6) and (7), respectively, as shown in (25) at the bottom of the page. It reveals that the distortion evaluation of a G_m-C filter can be easily accomplished by simple matrix algebra. These closed-form expressions compare favourably to others in the literature, demanding a much more cumbersome formulation [4], [5].

Let us now consider the case where the output summing structure of Fig. 1(a) also contributes distortion. In this case, the conceptual schematic of the filter output takes the form in Fig. 5, similar to that in Fig. 3 for the filter core. As above, the analysis of this circuit encompasses decomposition into a first- and a third-order schematics (shown, respectively, in Fig. 6(a) and (b)) which are solved one after the other to give

$$\begin{aligned} v_{O1} &= \mathbf{C}\mathbf{x}_1 + dv_I \\ v_{O3} &= \mathbf{C}\mathbf{x}_3 + h_3(\mathbf{C}\mathbf{x}_1^3 + dv_I^3 + v_{O1}^3) \end{aligned} \tag{26}$$

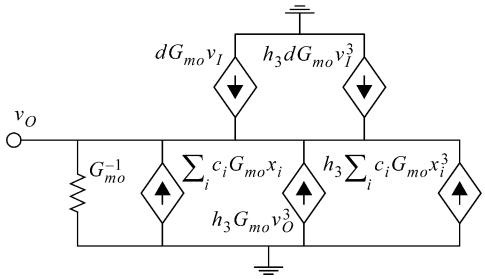

Fig. 5. Conceptual schematic of the output structure including nonlinearities.

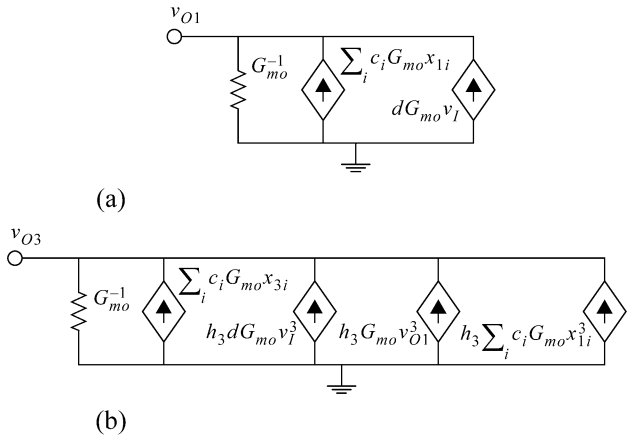

Fig. 6. First-order (a) and (b) third-order (b) circuits to evaluate the distortion of the output stage.

where $\mathbf{x}_1$ and $\mathbf{x}_3$ are obtained from (22) and (23). In these v_{O1} represents the linear part of the filter response, and v_{O3} the third-order nonlinear contribution. After some algebra, the third-order harmonic distortion of the filter and its intermodulation performance take the form in (27), shown at the bottom of the page, where terms $N_{HD_3}(\omega)$ and $N_{IM_3}(\omega_1, \omega_2)$, defined in (25), are due to the core of the filter.

As an illustration of the proposed distortion evaluation method, Fig. 7 shows in solid lines the calculated third-order intermodulation and harmonic distortion components of a fully balanced seventh-order low-pass Chebyshev filter with 10 MHz cut-off frequency. The filter uses a standard leap-frog structure

$$\begin{aligned} HD_3(\omega) &= \frac{h_3}{4}\left|\frac{\mathbf{G}(3\omega)(\mathbf{A}\mathbf{F}^{(3)}(\omega) + \mathbf{B}_G}{H(\omega)}\right|\rho^2 \equiv \frac{h_3}{4}\left|\frac{N_{HD_3}(\omega)}{H(\omega)}\right|\rho^2 \\ IM_3(2\omega_1 \pm \omega_2) &= \frac{3h_3}{4}\left|\frac{\mathbf{G}(2\omega_1 \pm \omega_2)(\mathbf{A}(\mathbf{F}^{(2)}(\omega_1) \bullet \mathbf{F}(\pm\omega_2)) + \mathbf{B}_G}{H(\omega_1)}\right|\rho^2 \equiv \frac{3h_3}{4}\left|\frac{N_{IM_3}(\omega_1,\omega_2)}{H(\omega_1)}\right|\rho^2 \end{aligned} \tag{25}$$

$$\begin{aligned} HD_3(\omega) &= \frac{h_3}{4}\left|\frac{N_{HD_3}(\omega) + \mathbf{C}\mathbf{F}^{(3)}(\omega) + H(\omega)^3 + d}{H(\omega)}\right|\rho^2 \\ IM_3(2\omega_1 \pm \omega_2) &= \frac{3h_3}{4}\left|\frac{N_{IM_3}(\omega_1,\omega_2) + \mathbf{C}(\mathbf{F}^{(2)}(\omega_1) \bullet \mathbf{F}(\pm\omega_2)) + H(\omega_1)^2 H(\omega_2) + d}{H(\omega_1)}\right|\rho^2 \end{aligned} \tag{27}$$

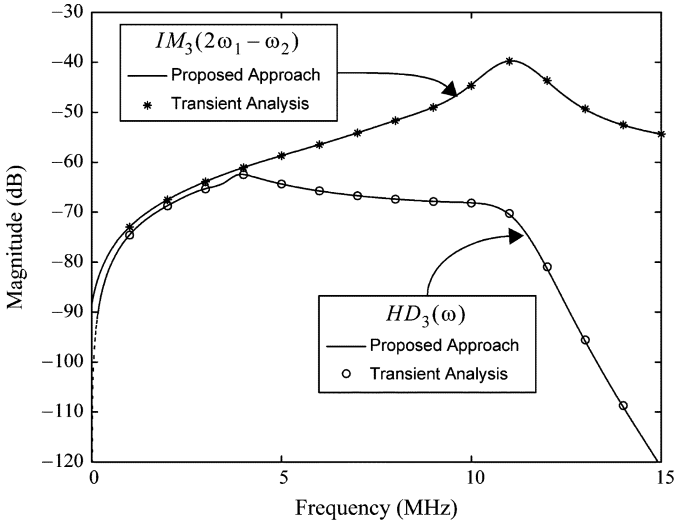

Fig. 7. Estimations of $IM_3(2\omega_1-\omega_2)$ and $HD_3(\omega)$. using transient analysis and the proposed method.

and it is assumed that all transconductors exhibit a third-order nonlinear term $h_3 = 0.08\,\mathrm{V}^{-2}$.

Calculations are made assuming that the filter is driven by input tones of 125 mV at different frequencies. The third-order intermodulation estimation assumes a 100 kHz offset frequency between the input tones. For comparison purposes, Fig. 7 includes also entries for the third-order intermodulation (asterisks) and harmonic distortion (circles) calculated at different input frequencies by means of conventional Fourier analysis of a transient response. As can be seen, both methods give approximately the same results, however, whereas the computational cost of the transient approach is 135 s cpu time, that of the proposed method is of only 0.6 s (data using a 1.8 GHz Pentium Mobile processor), i.e., more than two orders of magnitude lower.

V. Scaling of G_m-C Filters

This section presents analytic expressions to account for the impact of scaling on filter noise and distortion. This is worth doing because scaling is customarily employed for filter design [6], [12], [17], [18]. We consider only scaling operations which retain the frequency response, $H(\omega)$, required by the application. This excludes frequency scaling operations which are easily implemented by multiplying all filter capacitances by the same factor α_C [this makes $\tilde{\mathbf{E}} = \alpha_C\mathbf{E}$, $\tilde{\mathbf{B}}_\mathbf{C} = \alpha_C B_C$ and, thereafter, $\tilde{H}(s) = H(\alpha_C s)$] or by scaling all filter transconductances by α_G [this makes $\tilde{\mathbf{A}} = \alpha_G\mathbf{A}$, $\tilde{\mathbf{B}}_G = \alpha_\mathbf{G} B_G$ and, thereafter, $\tilde{H}(s) = H(s/\alpha_G)$].

In the foregoing analysis, filters are grouped into two categories. On the one hand, filters with all capacitors grounded excepting, perhaps, those connecting the integration nodes with the filter input (they are characterized by a diagonal matrix $\mathbf{E}$). On the other hand, filters which include floating capacitors between integration nodes.

Unless otherwise stated, if x denotes a given variable in the prototype system, $\tilde{x}$ represents the corresponding transformed variable.

A. Filters Without Floating Capacitors

Table I summarizes results for the three types of scaling considered herein. The second column shows the basic and derived matrix equations for each type of scaling. The third column includes comments regarding the effects of corresponding transformation on the noise and distortion performance of the filter.

A first scaling approach consists of multiplying each row of the state equation in (1) by a corresponding positive number, β_i. This transformation, denoted as *noise scaling* in Table I, modifies the local impedance at each node of the filter without altering their voltage swings. Hence, it does not affect the distortion behavior of the filter-interesting property that will be exploited later on.

The noise contributed to the output from the ith integration node in the scaled filter becomes $\overline{\tilde{U}^2_{no,i}} = \overline{U^2_{no,i}}/\beta_i$, whereas the sum of all transconductances driving the ith node of the filter scales as $\tilde{G}_{mi} = |\tilde{b}_i| + \sum_j |\tilde{a}_{ij}| = \beta_i G_{mi}$. It means that to reduce the noise contribution at node i by a factor $\beta_i > 1$, the total transconductance G_{mi} must be increased by the same factor. This increases the area occupation of the filter as well, because capacitances are also scaled by β_i.

For a given value of the total transconductance, $G_{m,tot} = \sum_i \tilde{G}_{mi} = \sum_i \beta_i G_{mi}$, there is an optimum set of scaling coefficients β_i, $i = 1,\ldots,n$, which minimizes the total noise contributed by the filter. After some calculations (detailed in Appendix I) it is found that such optimum set is obtained when all the diagonal elements of the transformed matrix $\tilde{\mathbf{W}}$ are identical, i.e.,

$$\tilde{W} \equiv \tilde{w}_{11} = \cdots = \tilde{w}_{nn} = \left[\sum_j \tilde{w}_{jj}^{1/2}\frac{G_{mj}}{G_{m,tot}}\right]^2 \tag{28}$$

which gives

$$\beta_{i,opt} = \frac{w_{ii}^{1/2}}{\sum_j w_{jj}^{1/2} G_{mj}} G_{m,tot}. \tag{29}$$

In this case, the total noise of the filter can be expressed as

$$\overline{\tilde{U}^2_{no}} = 2kT\xi\tilde{W}G_{m,tot}. \tag{30}$$

A special case of noise scaling is *power scaling* in which all the multiplying factors β_i take on the same value β and, hence, all capacitors and transconductors of the filter core are scaled by β. In this case, the total output noise value of the filter is transformed according to $\overline{\tilde{U}^2_{no}} = \overline{U^2_{no}}/\beta$, without affecting the distortion behavior. This fact will be used in Section VI to relate the total noise of the filter with its power consumption.

Consider now that scaling is made by multiplying column entries instead of row entries. This transformation is labelled *distortion scaling* in Table I where scaling factors are called γ_j, $j = 1,\ldots,n$. It affects the amplitude level of the voltages at the internal nodes of the filter and, therefore, modifies its distortion behavior. Actually, distortion improves for scaling factors $\gamma_j > 1$. However, this operation affects the noise behavior and defines a trade-off between noise and distortion. It is worth noting that matrix $\mathbf{G}$ remains unaltered after distortion scaling and so $\tilde{w}_{ii} = w_{ii}$. This fact will be exploited in the next section.

TABLE I
BASIC SCALING TRANSFORMATIONS

	Scaling Transformation[a]	Comments
Noise scaling	**Basic Eqs.** $\tilde{\mathbf{E}} = \mathbf{D}(\{\beta_i\})\mathbf{E}$ $\tilde{\mathbf{A}} = \mathbf{D}(\{\beta_i\})\mathbf{A}$ $\tilde{\mathbf{B}} = \mathbf{D}(\{\beta_i\})\mathbf{B}$ **Derived Eqs.** $\tilde{\mathbf{F}} = \mathbf{F}$ $\tilde{\mathbf{G}} = \mathbf{G}\mathbf{D}(\{\beta_i^{-1}\})$ $\tilde{w}_{ii} = w_{ii}/\beta_i^2$	It introduces local impedance scaling at each node of the filter, but does not alter their voltage swings. Hence, this transformation does not affect the distortion behavior of the filter, i.e., $\tilde{HD}_3(\omega) = HD_3(\omega)$ $\tilde{IM}_3(2\omega_1 \pm \omega_2) = IM_3(2\omega_1 \pm \omega_2)$ The noise contributed to the output from the i-th integration node in the scaled filter is given by $\overline{\tilde{U}^2_{no,i}} = \overline{U^2_{no,i}}/\beta_i = 2kT\xi\tilde{w}_{ii}\beta_i\left(\lvert b_i\rvert + \sum_j \lvert a_{ij}\rvert\right)$
Distortion scaling	**Basic Eqs.**[b] $\tilde{\mathbf{E}} = \mathbf{E}\mathbf{D}(\{\gamma_j\})$ $\tilde{\mathbf{A}} = \mathbf{A}\mathbf{D}(\{\gamma_j\})$ $\tilde{\mathbf{C}} = \mathbf{C}\mathbf{D}(\{\gamma_j\})$ **Derived Eqs.** $\tilde{\mathbf{F}} = \mathbf{D}(\{\gamma_j^{-1}\})\mathbf{F}$ $\tilde{\mathbf{G}} = \mathbf{G}$ $\tilde{w}_{ii} = w_{ii}$	It modifies the amplitude level of the voltages at the internal nodes of the filter and, therefore, modifies its distortion behavior: $\tilde{HD}_3(\omega) = \frac{h_3}{4}\left\lvert\frac{\mathbf{G}(3\omega)(\mathbf{A}\mathbf{D}(\{\gamma_j^{-2}\})\mathbf{F}^{(3)}(\omega) + \mathbf{B}_G)}{H(\omega)}\right\rvert\rho^2$ $\tilde{IM}_3(2\omega_1 \pm \omega_2) = \frac{3h_3}{4}\left\lvert\frac{\mathbf{G}(2\omega_1 \pm \omega_2)(\mathbf{A}\mathbf{D}(\{\gamma_j^{-2}\})(\mathbf{F}^{(2)}(\omega_1) \bullet \mathbf{F}(\pm\omega_2)) + \mathbf{B}_G)}{H(\omega)}\right\rvert\rho^2$ Noise behavior is also altered according to $\overline{\tilde{U}^2_{no,i}} = 2kT\xi\tilde{w}_{ii}\left(\lvert b_i\rvert + \sum_j \gamma_j\lvert a_{ij}\rvert\right)$
Similarity scaling	**Basic Eqs.** $\tilde{\mathbf{A}} = \mathbf{T}\mathbf{A}\mathbf{T}^{-1}$ $\tilde{\mathbf{B}} = \mathbf{T}\mathbf{B}$ $\tilde{\mathbf{C}} = \mathbf{C}\mathbf{T}^{-1}$ $\tilde{\mathbf{E}} = \mathbf{T}\mathbf{E}\mathbf{T}^{-1}$ **Derived Eqs.** $\tilde{\mathbf{F}} = \mathbf{T}\mathbf{F}$ $\tilde{\mathbf{G}} = \mathbf{G}\mathbf{T}^{-1}$ $\tilde{\mathbf{W}} = (\mathbf{T}^{-1})^{\mathrm{T}}\mathbf{W}\mathbf{T}^{-1}$	As in the distortion scaling transformation, this approach modifies both the noise and distortion behavior of the filter. For the case in which $\mathbf{T}$ is a diagonal matrix, $\mathbf{T} = \mathbf{D}(\{\delta_i\})$, the third order harmonic and intermodulation distortion of the filter take the form: $\tilde{HD}_3(\omega) = \frac{h_3}{4}\left\lvert\frac{\mathbf{G}(3\omega)(\mathbf{A}\mathbf{D}(\{\delta_i^2\})\mathbf{F}^{(3)}(\omega) + \mathbf{B}_G)}{H(\omega)}\right\rvert\rho^2$ $\tilde{IM}_3(2\omega_1 \pm \omega_2) = \frac{3h_3}{4}\left\lvert\frac{\mathbf{G}(2\omega_1 \pm \omega_2)(\mathbf{A}\mathbf{D}(\{\delta_i^2\})(\mathbf{F}^{(2)}(\omega_1) \bullet \mathbf{F}(\pm\omega_2)) + \mathbf{B}_G)}{H(\omega)}\right\rvert\rho^2$ and the noise contributed to the output from the i-th integration node is, $\overline{\tilde{U}^2_{no,i}} = 2kT\xi\tilde{w}_{ii}\delta_i\left(\lvert b_i\rvert + \sum_j (\lvert a_{ij}\rvert/\delta_j)\right)$

a. Function $\mathbf{D}(\cdot)$ recasts a given ordered set of coefficients into a diagonal matrix, e.g., given the coefficients $\{\beta_i\}$, $i = 1, \ldots, n$, $\mathbf{D}(\{\beta_i\}) = \mathbf{I}[\beta_1, \ldots, \beta_n]^{\mathrm{T}}$, where $\mathbf{I}$ is the $n \times n$ identity matrix.

b. Note that matrix $\mathbf{B}$ remains unscaled. Hence, the transformation $\tilde{\mathbf{E}} = \mathbf{E}\mathbf{D}(\{\gamma_j\})$ implies that the new grounded capacitances of the filter become $\tilde{C}_{jj} = \gamma_j C_{jj} + (\gamma_j - 1)C_{bj}$, according to the definition in (3).

A last option for filter scaling consists of applying a similarity transformation on the state-space representation in (1). A typical case, illustrated in Table I, corresponds to a diagonal transforming matrix $\mathbf{T}$ with coefficients δ_i. As in the previous case, this mapping carries on both noise and distortion modifications on the prototype filter, and a trade-off can be established as well: scaling factors $\delta_i > 1$ decrease the noise contribution but worsen distortion. This type of transformation is typically used to equalize and maximize the peak voltages at the input of the transconductors in the filter—this is done by means of a diagonal T matrix with coefficients $\delta_i = v_{max}/v_{peak,i}$, $i = 1, \ldots, n$, where v_{max} is the maximum input signal range of transconductors and $v_{peak,i} = \max_\omega(\lvert f_i(\omega)\rvert)$ are the peak values of each f_i defined in (5) (they usually occur near the passband of the filter) [17].

B. Filters With Floating Capacitors

The presence of floating capacitors between the integration nodes makes the matrix $\mathbf{E}$ non-diagonal. As a consequence, previous scaling operations cannot be applied in stand-alone manner. Otherwise the symmetry of $\mathbf{E}$ [see (3)] would be lost, the feedback and forward paths of the floating connections would be different and, consequently, they would be unrealizable with simple capacitors. To overcome this situation, scaling operations should be pair-wise applied so that symmetry of $\mathbf{E}$ is always restored after scaling.[5]

As an example, let us assume that a prototype filter with floating capacitors is scaled by a diagonal similarity transformation $\mathbf{T} = \mathbf{D}(\{\delta_i\})$. The non-diagonal components of matrix $\mathbf{E}$ change as $\tilde{e}_{ij} = (\delta_i/\delta_j)e_{ij}$, thus, breaking the symmetry for $\delta_i \neq \delta_j$. In order to restore this property and, hence, allow the use of floating capacitors as in the prototype filter, one possibility is to noise scale the filter (see Table I), in such a way that the relationship $\beta_j\delta_j^2 = \beta_i\delta_i^2$ is met for $i \neq j$, $i, j = 1, \ldots, n$, what guarantees that $\tilde{e}_{ij} = \tilde{e}_{ji}$. A similar procedure can be envi-

[5]Rigorously speaking, scaling could be performed in a single step by means of a similarity transformation with an orthogonal $\mathbf{T}$ matrix ($\mathbf{T}^{-1} = \mathbf{T}^{\mathrm{T}}$). However, from a synthesis perspective, it is more simple and intuitive to use two consecutive scaling operations.

sioned if, instead of noise scaling, a distortion scaling is applied for restoring $\mathbf{E}$ symmetry.

VI. Dynamic Range Optimization of General G_m-C Filters

We have seen that for a given total transconductance the noise of a G_m-C filter can be minimized by making all diagonal terms of matrix $\mathbf{W}$ identical. We have also seen that, by applying distortion scaling, the harmonic distortion and intermodulation performance can be improved while keeping the terms w_{ii} unaltered. Hence, an optimum noise-scaled filter will retain this feature after distortion scaling. This observation is at the core of a recently proposed procedure for dynamic range optimization of weakly nonlinear G_m-C filters under power dissipation constraints [6]. It consists of the consecutive application of noise and distortion optimizations on the prototype filter. However, this procedure presents two limitations. First, the noise and distortion contributions, as well as power consumption, of transconductors not accounted in matrix $\mathbf{A}$ are neglected. Indeed, transconductors assessed in matrix $\mathbf{B}$ are replaced by ideal current sources. This simplification precludes obtaining univocal solutions from the optimization procedure, as will be illustrated in the next section by means of an example. Second, distortion optimization is constrained by the condition that the noise generated at the filter core keeps unaltered. This condition reduces the design space of filter parameters and, consequently, may preclude that a global optimum is reached.

These drawbacks are overcome by the procedure presented in this section. Without loss of generality and to keep mathematics as simple as possible, let us assume that all transconductors in the filter share the same topology and linear range, and exhibit the same current efficiency, Γ; where this latter parameter is defined as the ratio between the transconductance and the biasing current of the cell [18], [19]. In this case, the total power consumption of the filter, P_{tot}, is proportional to the sum of all its transconductances, $G_{m,tot}$, as $P_{tot} = G_{m,tot}V_{DD}/\Gamma$, where V_{DD} is the power supply voltage of the filter [18]. A practical way of fulfilling this assumption is by implementing all transconductance values through the parallel connection of unitary transconductors.[6]

Let us assume that a generic fully balanced G_m-C filter with no output network (see Fig. 1(a)) has been, first, optimally noise scaled and, then, distortion and power scaled. In this case, taking into account Table I and applying a power scaling factor $\beta = \Gamma P_{tot}/(\overline{G}_{m,tot}V_{DD})$, the total noise of the filter for a total power consumption becomes

$$\overline{\tilde{U}_{no}^2} = 2kT\xi\tilde{W}\left[\sum_i\left(|\tilde{b}_i| + \sum_j \gamma_j|\tilde{a}_{ij}|\right)\right]^2 \frac{V_{DD}}{\Gamma P_{tot}} = 2kT\xi\tilde{W}\overline{G}_{m,tot}^2\frac{V_{DD}}{\Gamma P_{tot}} \tag{31}$$

[6]This is, indeed, a common practice among integrated circuit designers. By using multiple instances of a given transconductor, the design complexity is notably reduced and the robustness of the filter against variations of the technological process is improved. Using this strategy in combination with proper layout techniques, matching between transconductors is largely favoured and the tunability of the filter, simplified [20], [21].

where $\tilde{a}_{ij}$ and $\tilde{b}_i$ are the coefficients of the matrices $\tilde{\mathbf{A}}$ and $\tilde{\mathbf{B}}$ after optimum noise scaling, and $\overline{G}_{m,tot}$ is the sum of all the transconductances of the filter after distortion scaling. Useful for the foregoing analysis, $\overline{G}_{m,tot}$ can be also expressed as

$$\overline{G}_{m,tot} = \tilde{G}_{mb} + \sum_j \gamma_j \tilde{G}'_{mj} \tag{32}$$

where $\tilde{G}'_{mj}$ (respectively, $\tilde{G}_{mb}$) is the sum of the transconductances of all the transconductors with input at the jth node (respectively, filter input) of the optimum noise-scaled filter.[7]

Let us further assume, without loss of generality, that the distortion performance of the filter is evaluated by the third-order intermodulation. From Table I and assuming that input tones are close together ($\omega_1 \approx \omega_2 \approx \omega$), $I\tilde{M}_3$ at $2\omega_1 - \omega_2$ can be expressed as

$$I\tilde{M}_3(\omega) = \frac{3h_3}{4}\left|\frac{\tilde{\mathbf{G}}(\omega)(\tilde{\mathbf{A}}\mathbf{D}(\{1/\gamma_j^2\})(\mathbf{F}^{(2)}(\omega)\bullet\mathbf{F}(-\omega)) + \tilde{\mathbf{B}}_G}{H(\omega)}\right|\rho^2 \tag{33}$$

where $\tilde{\mathbf{G}}$, see definition in (7), is obtained after optimum noise scaling. Equation (33) can be also written as

$$I\tilde{M}_3(\omega) = \frac{3h_3}{4}\left|Y + \sum_j \frac{X_j}{\gamma_j^2}\right|\frac{\rho^2}{|H(\omega)|} \equiv \frac{3h_3}{4}|M|\frac{\rho^2}{|H(\omega)|} \tag{34}$$

where coefficients X_j and Y, both independent of γ_j, are defined as

$$X_j = \sum_i \tilde{g}_i(\omega)\tilde{a}_{ij}f_j^2(\omega)f_j(-\omega)$$
$$Y = \tilde{\mathbf{G}}(\omega)\tilde{\mathbf{B}}_G. \tag{35}$$

The maximum power at the output of the filter, P_{max}, for a peak intermodulation distortion value, $I\tilde{M}_{3,max}(\omega)$, can be obtained from (34) as

$$P_{max} = \frac{4}{3}\frac{I\tilde{M}_{3,max}(\omega)}{h_3|M|}|H(\omega)|^3 \tag{36}$$

from where the dynamic range of the filter (see footnote 1) can be calculated, using (31), as

$$DR = \frac{\Gamma}{\xi h_3 V_{DD}} \times \frac{|H(\omega)|^3}{\tilde{W}\bar{G}_{m,tot}^2|M|}\frac{2}{3}\frac{I\tilde{M}_{3,max}(\omega)}{kT}P_{tot}. \tag{37}$$

This expression can be recast as

$$DR = T_{DR} \times S_{DR} \times \frac{2}{3}\frac{I\tilde{M}_{3,max}(\omega)}{kT}P_{tot} \tag{38}$$

where $T_{DR} \equiv \Gamma/(\xi h_3 V_{DD})$ is an adimensional number, which depends on the particular transconductor implementation used in the filter, and $S_{DR} \equiv |H(\omega)|^3/(\tilde{W}\bar{G}_{m,tot}^2|M|)$ depends on the filter structure. Parameter T_{DR} gives a measure on how large the dynamic range of a filter can be for a given power dissipation

[7]In this section and the following, if x denotes a variable or coefficient of the original prototype, $\bar{x}$ refers to the corresponding variable or coefficient of the optimally noise scaled filter.

and distortion performance. Hence, it can be used as a figure of merit for comparing transconductor implementations.

Equation (38) also shows that for a given power consumption (P_{tot}), maximum tolerated distortion ($I\tilde{M}_{3,max}(\omega)$) and selected transconductor topology (T_{DR}), the optimization of the filter dynamic range implies maximizing S_{DR}. As $|H(\omega)|$ remains unaltered after scaling, the only scaling-dependent factor in S_{DR} is $\tilde{W}\bar{G}^2_{m,tot}|M|$, which we define as a cost function in the dynamic range optimization procedure

$$F_C = \tilde{W}\bar{G}^2_{m,tot}|M|. \tag{39}$$

Clearly, to optimize the dynamic range of a filter, F_C must be minimized. The minimum of F_C is calculated by setting $\partial F_C/\partial\gamma_j = 0$, which after some algebra obtains the set of equations

$$\begin{aligned}&\mathrm{Re}\left[M^\dagger \frac{X_1}{\gamma_1^2}\right]\\ &= \frac{|M|^2}{\bar{G}_{m,tot}}\gamma_1\tilde{G}'_{m1}\ldots\mathrm{Re}\left[M^\dagger\frac{X_n}{\gamma_n^2}\right]\\ &= \frac{|M|^2}{\bar{G}_{m,tot}}\gamma_n\tilde{G}'_{mn}\end{aligned} \tag{40}$$

where $M^\dagger$ is the conjugate of M and $\mathrm{Re}(\cdot)$ extracts the real part of the argument. Summing the left-hand terms of the above n equations, on the one hand, and the right-hand terms, on the other, the following two relationships are obtained:

$$\begin{aligned}\sum_j \mathrm{Re}\left[M^\dagger\frac{X_j}{\gamma_j^2}\right] &= |M|^2 - \mathrm{Re}(M^\dagger Y)\\ \frac{|M|^2}{\bar{G}_{m,tot}}\sum_j\gamma_j\tilde{G}'_{mj} &= |M|^2\left(1-\frac{\tilde{G}_{mb}}{\bar{G}_{m,tot}}\right)\end{aligned} \tag{41}$$

from where, equating the results and using (40), the optimum distortion-scaling coefficients γ_j can be calculated by recursively solving the expression

$$\gamma_j^3 = \frac{\tilde{G}_{mb}}{\tilde{G}'_{mj}}\frac{\mathrm{Re}(M^\dagger X_j)}{\mathrm{Re}(M^\dagger Y)} \tag{42}$$

using the definition of M in (34). With these γ_j values, the absolute minimum for F_C becomes

$$F_C = \tilde{W}\sqrt{\mathrm{Re}(M^\dagger Y)\frac{\bar{G}^5_{m,tot}}{\tilde{G}_{mb}}}. \tag{43}$$

Note that if input transconductors are not accounted for in the above analysis, which is the situation considered in [6], coefficients Y and $\tilde{G}_{mb}$ are null and (43) becomes indeterminate.[8]

[8]By removing the *effects* of input transconductors on distortion and noise, they are assumed to perform as perfect voltage-to-current converters. In essence, these ideal converters play the same role as the input current-controlled current sources used in [6], i.e., to inject signal into a current-input filter. Assuming that $\mathbf{B}$ has no capacitive components, i.e., $\mathbf{B}_C$ is a null vector, the driving signal of the current-input filter takes in our model the form $\mathbf{B}v_I$. In the case of [6], such driving signal is simply given by $\mathbf{B}\mathbf{i}_I$. Obviously, the dimensionality of matrix $\mathbf{B}$ in both procedures is different but, from the point of view of optimizing the dynamic range of the current-input filter, defined by matrix $\mathbf{A}$ and $\mathbf{E}$, this is irrelevant.

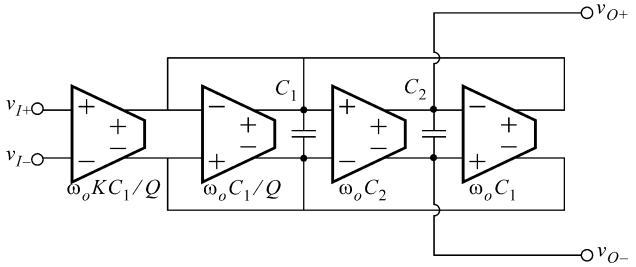

Fig. 8. Fully differential G_m-C biquadratic section.

This reveals that there is an infinite number of solutions that achieve the same dynamic range for a given power dissipation, and not a single solution as stated in [6]. It is to be understood that by including the effects of input transconductors on distortion and noise, the optimization algorithm finds the necessary constraint to achieve a single and univocal solution.

It is also worth mentioning that the dynamic range optimization may result in a non-unity distortion-scaling coefficient for the output node of the filter, i.e., if the output is taken from node n, coefficient γ_n will more likely be $\gamma_n \neq 1$. This implies that vector $\mathbf{C}$ becomes non-unitary, however, there is no need to add an amplification output stage to the filter (see Fig. 1) to guarantee an optimum dynamic range. Instead, the output of the filter could be directly taken from node n. Note that any potential output network will ideally scale the output noise and desired signal power by the same factor while retaining the distortion performance of the filter core. Therefore, the dynamic range will remain unaltered after amplification.

Finally, note that the optimization process described above is restricted to a single operating frequency. Therefore, such frequency must be carefully chosen so that it corresponds to the worst-case dynamic range of the filter. This can be done by a previous analysis on the noise and distortion dependence with frequency through (10) and (25).

VII. Case Study: Biquadratic Sections

As a case of study, the procedure in the previous section is herein applied to the biquadratic section of Fig. 8. In the following analysis, transconductor-dependent parameters have been derived from a simple folded-cascode topology, designed in a 0.13 μm CMOS technology at a power supply of 3.3 V. They are $h_3 = 0.08\,\mathrm{V}^{-2}$, $\xi = 8.3$, and $\Gamma = 0.165\,\mathrm{V}^{-1}$, giving $T_{DR} = 0.075$. Using these transconductors, a low-pass filter with cut-off frequency at $f_0 = 10.7$ MHz has been designed. The power consumption of this filter is $P_{tot} = 40$ mW.

Using the extended state-space representation of Section II, the biquad in Fig. 8 can be described by the matrices

$$\begin{aligned}\mathbf{A} &= \begin{bmatrix}-\frac{\omega_o C_1}{Q} & -\omega_o C_1\\ \omega_o C_2 & 0\end{bmatrix}\\ \mathbf{B} &= \begin{bmatrix}K\frac{\omega_o C_1}{Q}\\ 0\end{bmatrix}\\ \mathbf{C} &= [0\quad 1]\\ \mathbf{E} &= \begin{bmatrix}C_1 & 0\\ 0 & C_2\end{bmatrix}\\ d &= 0\end{aligned} \tag{44}$$

where vector $\mathbf{C}$ selects the low-pass output voltage (integration node 2) of the biquadratic section. Using (4), the input–output transfer function $H(s)$ can be obtained as

$$H(s) = \frac{\omega_o K/Q}{s^2 + (\omega_o/Q) + \omega_o^2} \tag{45}$$

where Q is the quality factor of the filter, and K determines the voltage gain of the biquad. Additionally, the total transconductance of the biquad is,

$$G_{m,tot} = (C_2 Q + C_1(1 + K + Q))\frac{\omega_o}{Q} \tag{46}$$

the total output noise mean-squared value of the filter is given by

$$\overline{U_{no}^2} = kT\xi\left(\frac{(1+K+Q)}{C_1} + \frac{(1+Q^2)}{C_2 Q}\right) \tag{47}$$

and the matrix $\mathbf{W}$, defined in (12), can be obtained by solving the generalized Lyapunov equation in (13), as

$$\mathbf{W} = \frac{1}{\omega_o}\begin{bmatrix} Q/\left(2C_1^2\right) & 1/(2C_1C_2) \\ 1/(2C_1C_2) & (1+Q^2)/\left(2C_2^2 Q\right) \end{bmatrix} \tag{48}$$

As noted in Section V, there is an optimum noise scaling transformation which minimizes the total noise contributed by the biquad for a given amount of total transconductance. Such transformation uses the scaling factors (29),

$$\begin{aligned} \beta_{1,opt} &= \frac{\alpha Q}{C_1\omega_o} \\ \beta_{2,opt} &= \frac{\alpha\sqrt{1+Q^2}}{C_2\omega_o} \end{aligned} \tag{49}$$

where

$$\alpha = \frac{G_{m,tot}}{(1+K+Q+\sqrt{1+Q^2})} \tag{50}$$

which give, using (30), the following expression for $\overline{\tilde{U}_{no}^2}$:

$$\overline{\tilde{U}_{no}^2} = \frac{kT\xi\omega_o G_{m,tot}}{\alpha^2 Q}. \tag{51}$$

It is worth noting that $\overline{\tilde{U}_{no}^2}$ depends inversely on $G_{m,tot}$. The above transformation modifies the state-space matrix description as

$$\begin{aligned} \tilde{\mathbf{A}} &= \alpha\begin{bmatrix} -1 & -Q \\ \sqrt{1+Q^2} & 0 \end{bmatrix} \\ \tilde{\mathbf{B}} &= \alpha\begin{bmatrix} K \\ 0 \end{bmatrix} \\ \tilde{\mathbf{C}} &= [0 \quad 1] \\ \tilde{\mathbf{E}} &= \frac{\alpha}{\omega_o}\begin{bmatrix} Q & 0 \\ 0 & \sqrt{1+Q^2} \end{bmatrix}\tilde{d} = 0 \end{aligned} \tag{52}$$

and the value at the diagonal of matrix $\tilde{\mathbf{W}}$ now amounts $\tilde{W} = \omega_o/(2\alpha^2 Q)$.

Fig. 9 illustrates the effect of noise scaling on $\overline{\tilde{U}_{no}^2}$ as a function of the scaling coefficient β_1 for different quality factors of the biquad. In this figure, the second scaling coefficient, β_2, is constrained by keeping the total transconductance unaltered after the transformation. Additionally, it has been assumed that $K = 1$ and $C_1 = C_2$ in the original design. As can be seen, for every Q, $\overline{\tilde{U}_{no}^2}$ reaches a minimum value at $\beta_{1,opt}$ (displayed by circles in Fig. 9).

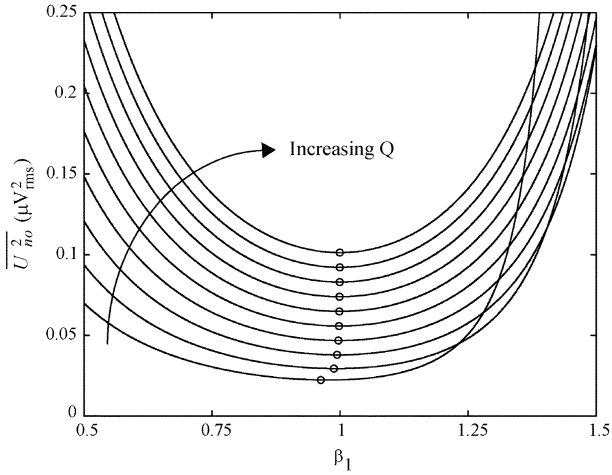

Fig. 9. Noise versus β_1 for the biquadratic section. The quality factor Q sweeps from 2 to 20 at steps of 2.

Fig. 10 illustrates the distortion performance at the low-pass output of the biquad. It shows the third-order harmonic distortion measured at 3ω as function of the input angular frequency, ω, [Fig. 10(a)]; and the third-order intermodulation distortion evaluated at $2\omega_1 - \omega_2$, assuming that both tones are very close together, so that $\omega_1 \approx \omega_2 \approx \omega$ [Fig. 10(b)]. The figures have been obtained for $Q = 5$ and $K = 1$ after a distortion scaling of the state-space matrix representation in (52) using coefficient γ_1 as sweeping parameter and setting $\gamma_2 = 1$. As can be seen from both figures, the third-order intermodulation distortion dominates over the third-order harmonic distortion and reaches a local maximum close to the cut-off frequency of the biquad. Interestingly enough, the third-order harmonic distortion exhibits notches which depend on the particular choice of the scaling parameters γ_1 and γ_2. This is better observed in Fig. 11(a), which represents the third-order harmonic distortion for an input tone at ω_0 as function of the scaling parameters γ_1 and γ_2. Indeed, it can be analytically demonstrated that the HD_3 notch occurs along the line $\gamma_1 = \sqrt{3}\gamma_2$, as can be observed in the figure. Together, the plot shows that distortion tends to diminish for large values of γ_1 and γ_2. This is also observed on the graphics for the third-order intermodulation distortion of Fig. 11(b). Increasing γ_1 and γ_2 to reduce the distortion response of the biquad implies, however, an increase on the output noise contribution, according to the expressions in Table I. This suggests a trade-off on the dynamic range of the filter, whose optimum value can be deduced by following the procedure in Section VI.

Considering that the distortion performance of the filter is evaluated by the third-order intermodulation component close to the cut-off frequency of the filter, ω_0, the maximum of the dynamic range is found by minimizing the cost function

$$F_C = \tilde{W}\bar{G}_{m,tot}^2 K\sqrt{1 + K^4Q^2\left\{\frac{1}{\gamma_1^2} + \frac{1}{\gamma_1^2}\right\}^2} \tag{53}$$

where $\bar{G}_{m,tot} = \alpha(K + \gamma_2 Q + \gamma_1(1+\sqrt{1+Q^2}))$. Taking into account that coefficients X_j and Y defined in (35) take the form

$$X_1 = K^3Q \qquad X_2 = K^3Q \qquad Y = -jK \tag{54}$$

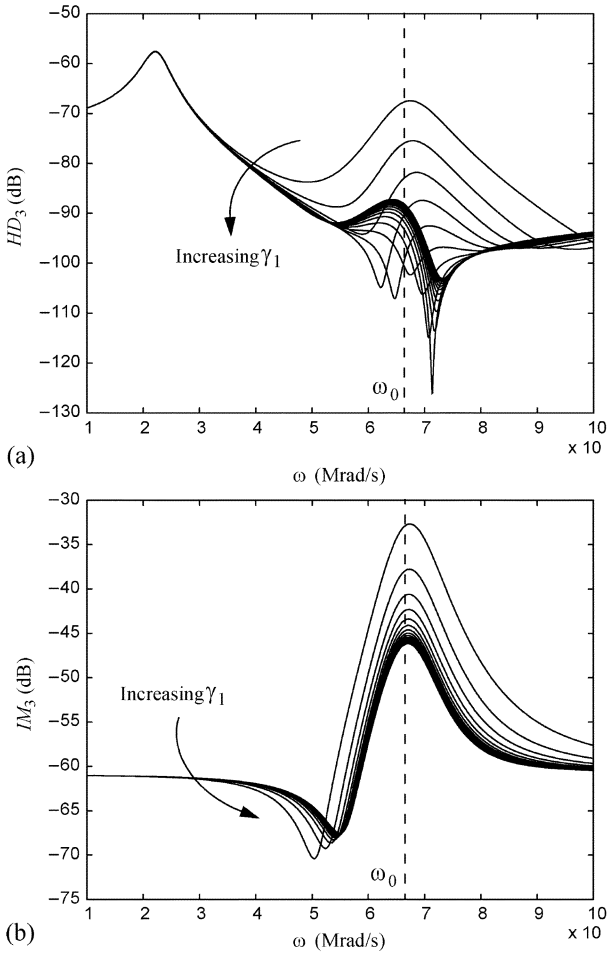

Fig. 10. Distortion performance in terms of the input frequency: (a) third-order harmonic distortion; (b) third-order intermodulation distortion. Scaling parameter γ_1 ranges from 0.5 to 5.0 at steps of 0.25.

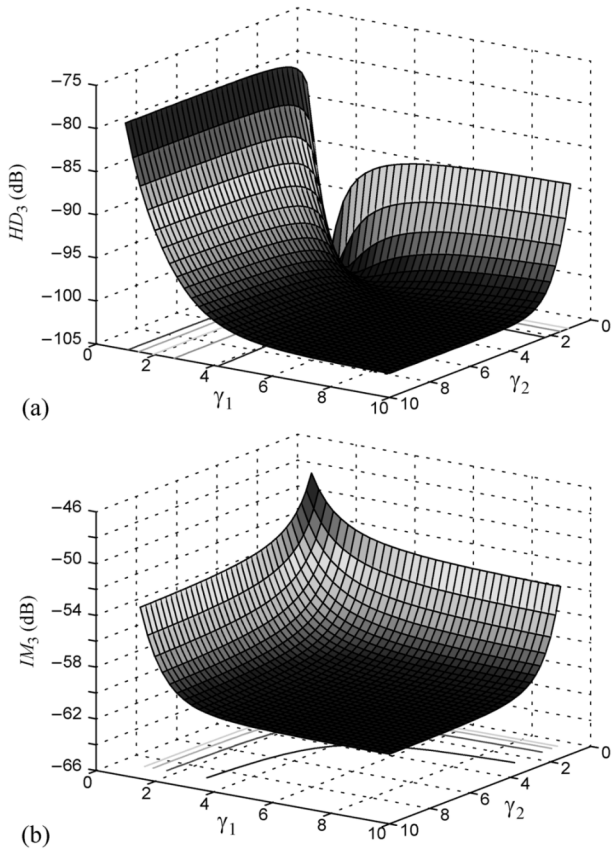

Fig. 11. Distortion performance for input tones close to the cut-off frequency of the filter in terms of the distortion scaling parameters γ_1 and γ_2 for $Q = 5$ and $K = 1$: (a) Third-order harmonic distortion; (b) third-order intermodulation distortion. Parameters γ_1 and γ_2 vary from 1.0 to 10.0 at steps of 0.25.

it can be found, applying (42), that the optimum values of the scaling factors γ_1 and γ_2 for $Q \gg 1$ values amount

$$\gamma_1 \approx \gamma_2 \approx (2Q)^{1/5} K \tag{55}$$

from where F_C can be approximated as $F_C \approx 4K^3 Q(1+Q)\omega_o$ and, finally, the optimum dynamic range of the biquadratic section can be expressed as

$$DR \approx \frac{I\tilde{M}_{3,max}(\omega_o)}{6kTQ(1+Q)\omega_o} T_{DR} P_{tot}. \tag{56}$$

Note that it happens to be inversely proportional to Q^2, contrarily to what it is stated in [1], [2], where the dynamic range is claimed to depend inversely on Q. It is also possible to express the dynamic range in (56) in terms of the total capacitance of the biquad, C_{tot}, after the optimization process. Assuming that Q is large enough, it can be found that $C_{tot} \approx G_{m,tot}/\omega_0$, from where, using the definition of T_{DR} in the previous section, the optimum dynamic range of the biquadratic section can be written as

$$DR \approx \frac{I\tilde{M}_{3,max}(\omega_o)}{6kTQ(1+Q)\omega_o \xi h_3} C_{tot} \tag{57}$$

and, hence, directly proportional to C_{tot}.

Fig. 12 shows the dynamic range of the biquad versus γ_1 and γ_2 for $Q = 5$, $K = 1$, and assuming a maximum intermodulation level of $IM_3(\omega_0) = -40$ dB. As it can be seen the maximum *DR*, which approximately amounts 57 dB, is obtained for the γ_1 and γ_2 values in (55). This is an improvement of 0.2 dB as compared to the dynamic range obtained from the distortion unscaled filter ($\gamma_1 = \gamma_2 = 1$). On the other hand, Fig. 13 shows the peak dynamic range versus Q for the same level of distortion. Note that the deviation between the exact expression, obtained by replacing (53) into (37), and the approximation in (56) tends to reduce as long as Q increases. In the same figure, results from transistor-level simulations of the biquad using the unitary transconductor previously designed have been included. As can be seen there is a good agreement among these results and the theoretical ones, thus confirming that *DR* is inversely proportional to the square of Q.

Fig. 14 compares the intermodulation performance a biquadratic section with $Q = 5$ obtained by transistor-level simulation and Fourier analysis, to that derived from the matrix methods proposed in this paper. In both cases, the filter has been excited with two tones separated 100 kHz and amplitude $\rho = 125$ mV. As can be seen, the deviation between both curves is lower than 1 dB. Regarding noise, the transistor-level design achieves a total output noise of $188.7\,\mu\mathrm{V_{rms}}$ whereas the

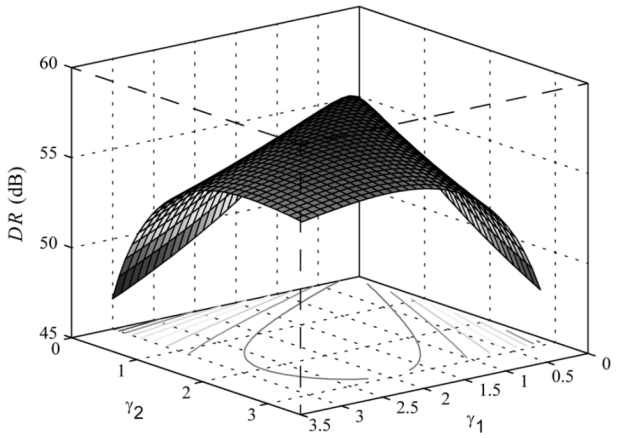

Fig. 12. *DR* versus γ_1 and γ_2 of the biquadratic section.

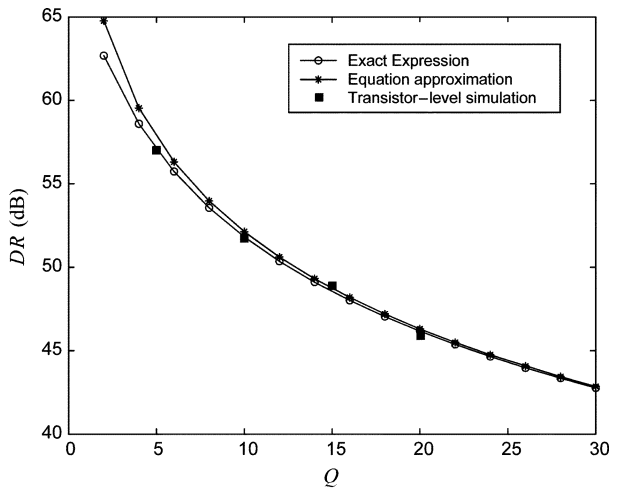

Fig. 13. *DR* versus Q for the biquadratic section.

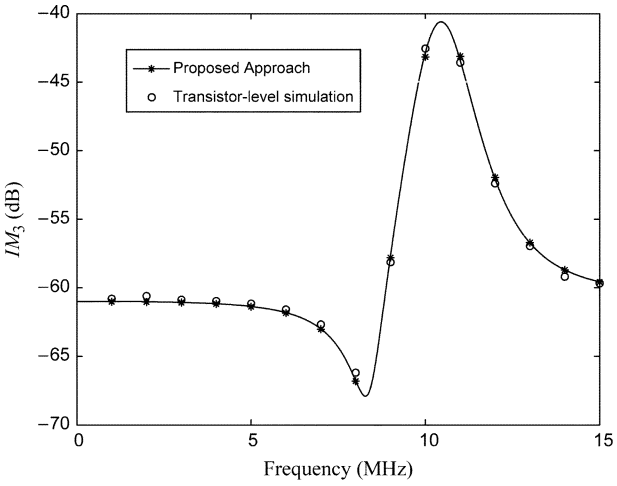

Fig. 14. Intermodulation over the frequency of a biquadratic section for two tones of 125 mV.

estimation obtained with the proposed approach is $187\ \mu\mathrm{V_{rms}}$. This represents a 0.9% deviation.

TABLE II
RESULTS OF THE PROPOSED OPTIMIZATION TECHNIQUE IN A CURRENT-INPUT BIQUAD

	Before	After
$\overline{\tilde{U}^2_{no}}$	$\frac{kT\xi(1+r)^2(1+Q)\omega_o}{rG_{m,tot}}$	$\frac{4kT\xi(2+3Q)\omega_o}{3G_{m,tot}}\gamma_2^2$
$IM_3(\omega_0)$	$\frac{3}{2}h_3K^2Q\rho^2$	$\frac{1}{2}h_3\frac{K^2(1+3Q)}{\gamma_2^2}\rho^2$
$\frac{DR}{T_{DR}P_{tot}}$	$\frac{2}{3}\frac{I\tilde{M}_{3,max}(\omega_o)}{kTQ(1+Q)\omega_o}\frac{r}{(1+r)^2}$	$\frac{3}{2}\frac{I\tilde{M}_{3,max}(\omega_o)}{kT(1+3Q)(2+3Q)\omega_o}$

To conclude this section, Table II compares the most relevant biquad parameters before and after applying the proposed dynamic range optimization. In this table, similar to [6], the influences of the input transconductor on noise and distortion have been neglected. This is done, first, to highlight the limitations of the approach in [6] and, second, to show that the proposed optimization procedure also holds for current-mode filters. A high Q value has been assumed in the calculations. The prototype design is a generic biquadratic section in which the capacitance ratio, $r = C_2/C_1$, can take an arbitrary value. Comparing both columns in Table II, it can be seen that the case $r = 1$ in the prototype filter obtains a *DR* very close to the optimum. On a related note, the second column of Table II shows that there is an infinite number of solutions which exhibit optimum dynamic range; each of them with a different noise and distortion behavior depending on the particular value of parameter γ_2. Using the same transconductor described above and assuming $Q = 5$, the optimum *DR* is found to be 57.6 dB. This is about 15% in linear scale higher than that previously calculated, however, it must be noted that now the effects of the input transconductor has been ignored. Using the methodology proposed in [6], the same optimum dynamic range value is obtained, however, only a single solution is provided, namely, that corresponding to $\gamma_2 = 1 + 1/(6Q)$. This particular solution is that which keeps noise constant during distortion optimization.

VIII. CONCLUSION

This paper presents a synthesis procedure to maximize the *DR* of continuous-time fully differential G_m-C filters. It presents fast methods to evaluate noise and distortion performances of filters using dot matrix representations, as well as a throughout discussion on the influence of amplitude and impedance scaling on them. Using these methods, an analytical procedure for the optimization of generic weakly nonlinear G_m-C filters for a given power consumption is presented. It shows that the dynamic range of G_m-C filters depends both on the selected transconductor topology and the high-level dimensioning of the filter, and that this latter can be optimized independently from the former by minimizing a simple cost function. A figure of merit to compare different transconductor structures is also proposed. The presented techniques have been

particularized to a simple biquadratic section and validated by electrical simulations of a transistor-level implementation. The analysis reveals that for a biquad with quality factor, Q, the optimum dynamic range is inversely proportional to Q^2, contrarily to what it is stated in previous publications.

APPENDIX

After noise scaling, the total transconductance of the filter, $G_{m,tot} = \sum_i G_{mi}$, is transformed into $\tilde{G}_{m,tot} = \sum_i \beta_i G_{mi}$. From this latter expression, the value of an arbitrary scaling coefficient, say β_n, can be related to the other ones, β_j, $j = 1, \ldots, n-1$, by the equation

$$G_{mn}\beta_n = \tilde{G}_{m,tot} - \sum_{j=1}^{n-1} \beta_j G_{mj}. \tag{58}$$

Taking into account (14) and Table I, the set of scaling coefficients β_i which minimizes the total noise contributed by the filter for a given amount of total transconductance $G_{m,tot}$ is obtained by solving the equations

$$\frac{\partial}{\partial \beta_i}\left[\frac{\overline{\tilde{U}_{no}^2}}{2kT\xi}\right] = \frac{\partial}{\partial \beta_i}\left[\sum_{j=1}^{n-1}\left(\frac{w_{jj}G_{mj}}{\beta_j}\right) + \frac{w_{nn}G_{mn}}{\beta_n}\right] = 0 \tag{59}$$

for $i = 1, \ldots, n$. Taking into account (58) and the constraint $\tilde{G}_{m,tot} = G_{m,tot}$, solving (59) gives

$$w_{ii}/\beta_i^2 = w_{nn}/\beta_n^2 = \overline{\tilde{U}_{no}^2}/(2kT\xi G_{m,tot}) \tag{60}$$

which is equivalent to set $\tilde{W} \equiv \tilde{w}_{11} = \ldots = \tilde{w}_{nn}$. From (60), the optimum β_i values are then obtained as

$$\beta_{i,opt} = \frac{w_{ii}^{1/2}}{\sum_j w_{jj}^{1/2} G_{mj}} G_{m,tot} \tag{61}$$

as stated in (29).

REFERENCES

[1] G. Groenewold, "The design of high dynamic range continuous-time integratable bandpass filters," *IEEE Trans. Circuits Syst.*, vol. 38, no. 8, pp. 838–852, Aug. 1991.

[2] G. Efthivoulidis, L. Toth, and Y. P. Tsividis, "Noise in G_m-C filters," *IEEE Trans. Circuits Syst. II, Analog Digit. Signal Process.*, vol. 45, no. 3, pp. 295–302, Mar. 1998.

[3] S. Koziel, R. Schaumann, and X. Haiqiao, "Analysis and optimization of noise in continuous-time OTA-C filters," *IEEE Trans. Circuits Syst. I, Reg. Papers*, vol. 52, no. 6, pp. 1086–1094, Jun. 2005.

[4] A. S. Korotkov and D. V. Morozov, "Nonlinear distortion analysis of G_m-C filters in frequency domain," in *Proc. 1st IEEE Int. Conf. Circuits Syst. Commun.*, St. Petersburg, Russia, 2002, pp. 58–61.

[5] P. Wambacq, G. Gielen, P. Kinget, and W. Sansen, "High-frequency distortion analysis of analog integrated circuits," *IEEE Trans. Circuits Syst. II, Analog Digit. Signal Process.*, vol. 46, no. 3, pp. 335–345, Mar. 1999.

[6] Y. Palaskas and Y. Tsividis, "Dynamic range optimization of weakly nonlinear, fully balanced, G_m-C filters with power dissipation constraints," *IEEE Trans. Circuits Syst. II, Analog Digit. Signal Process.*, vol. 50, no. 10, pp. 714–727, Oct. 2003.

[7] J. Chen, E. Sanchez-Sinencio, and J. Silva-Martinez, "Frequency-dependent harmonic distortion analysis of a linearized cross-coupled CMOS OTA and its application to OTA-C filters," *IEEE Trans. Circuits Syst. I, Reg. Papers*, vol. 53, pp. 499–510, Mar. 2006.

[8] Z. Zhang, A. Celik, and P. P. Sotiriadis, "State-space harmonic distortion modelling in weakly nonlinear, fully balanced G_m-C filters—A modular approach resulting in closed-form solutions," *IEEE Trans. Circuits Syst. I, Reg. Papers*, vol. 53, no. 1, pp. 48–59, Jan. 2006.

[9] A. Celik, Z. Zhang, and P. P. Sotiriadis, "A state-space approach to intermodulation distortion estimation in fully balanced bandpass G_m-C filters with weak nonlinearities," *IEEE Trans. Circuits Syst. I, Reg. Papers*, vol. 54, pp. 829–844, Apr. 2007.

[10] M. Schetzen, *The Volterra and Wiener Theories of Nonlinear Systems*. Malabar, FL: Krieger, 1980.

[11] Y. Tsividis, "Integrated continuous-time filter design—An overview," *IEEE J. Solid-State Circuits*, vol. 29, no. 3, pp. 166–176, Mar. 1994.

[12] S. Pavan and Y. Tsividis, *High Frequency Continuous Time Filters in Digital CMOS Process.*. Boston, MA: Kluwer Academic, 2000.

[13] G. Groenewold, "Noise and group delay in active filters," *IEEE Trans. Circuits Syst. I, Reg. Papers*, vol. 54, no. 7, pp. 1471–1480, Jul. 2007.

[14] V. Mehrmann and T. Stykel, , P. Benner, V. Mehrmann, and D. Sorensen, Eds., "Balanced truncation model reduction for large-scale systems in descriptor form," in *Dimension Reduction of Large-Scale Systems, Lecture Notes in Computational Science and Engineering*. Berlin/Heidelberg, Germany: Springer-Verlag, 2005, vol. 45, pp. 83–115.

[15] C. S. Hsu, U. B. Desai, and R. J. Darden, "Reduction of large-scale systems via generalized gramians," in *Proc. 22nd IEEE Conf. Decision and Control*, Dec. 1983, vol. 22, no. 1, pp. 1409–1410.

[16] F. F. Fernandez-Bootello and M. Delgado-Restituto, "Dynamic range optimization of continuous-time G_m-C filters," presented at the IEEE ECCTD 2005, Cork, Ireland, Aug. 2005.

[17] R. Gregorian and G. C. Temes, *Analog MOS Integrated Circuits for Signal Processing.*. New York: Wiley, 1986.

[18] F. Behbahani, T. Weeguan, A. Karimi-Sanjaani, A. Roithmeier, and A. A. Abidi, "A broad-band tunable CMOS channel-select filter for a low-IF wireless receiver," *IEEE J. Solid-State Circuits*, vol. 35, no. 4, pp. 476–489, Apr. 2000.

[19] R. Castello, F. Montecchi, F. Rezzi, and A. Baschirotto, "Low-voltage analog filters," *IEEE Trans. Circuits Syst. I, Fundam. Theory Applicat.*, vol. 42, no. 11, pp. 827–840, Nov. 1995.

[20] V. Gopinathan *et al.*, "Design considerations for high-frequency continuous-time filters and implementation of an antialiasing filter for digital video.," *IEEE J. Solid-State Circuits*, vol. 25, no. 6, pp. 1368–1378, Jun. 1990.

[21] V. Gopinathan *et al.*, "Design considerations and implementation of a programmable high-frequency continuous-time filter and variable-gain amplifier in submicrometer CMOS," *IEEE J. Solid-State Circuits*, vol. 34, no. 12, pp. 1698–1707, Dec. 1999.

Juan Francisco Fernández-Bootello was born in Seville, Spain, in 1976. He received the physics degree in 1999 and the electronic engineering degree in 2004 from the University of Seville. In 2000 he started to work in the Microelectronics Institute of Seville (IMSE) toward the Ph.D. degree in the group of analog and mixed-signal integrated circuits.

Since 2006, he is working for AnaFocus, Seville, as a mixed-signal designer. His research is focused on the design of high-frequencies continuous-time filters and mixed-signal circuits.

Manuel Delgado-Restituto (M'96) received the Ph.D. degree in physics from the University of Seville, Spain, in 1996.

In 1990, he joined the research staff of the Institute of Microelectronics of Seville (IMSE-CNM, CSIC). Since 1998, he occupies a permanent position as a tenured scientist of the Spanish Council for Scientific Research (CSIC). He has research interests in the design of analog and mixed-signal VLSI circuits for nonlinear signal processing, including vision chips, neuro-fuzzy controllers, and chaotic circuits for communications. He has also interest in the design and modelling of integrated circuits for wireless and power-line communication systems and the design for

reusability of analog and mixed-signal circuit blocks. He has authored or coauthored more than 80 international scientific publications and has been involved in many National and European R&D projects.

Dr. Delgado-Restituto was the 2007 Technical Program Co-Chairman of the European Conference on Circuit Theory and Design. He served as an Associate Editor of the IEEE TRANSACTIONS ON CIRCUITS AND SYSTEMS II—EXPRESS BRIEFS during 2006 and 2007, and currently serves in the Editorial Board of the IEEE TRANSACTIONS ON CIRCUITS AND SYSTEMS I—REGULAR PAPERS.

Ángel Rodríguez-Vázquez (M'80–SM'95–F'96) received the Ph.D. degree in physics-electronics in 1983.

He is a Full Professor of Electronics at the University of Seville. He founded and headed a research unit on High-Performance Analog and Mixed-Signal VLSI Circuits of the Institute of Microelectronics of Seville (IMSE-CNM). His team made pioneering R&D activities on bio-inspired microelectronics, including vision chips and neuro-fuzzy interpolators and controllers. His team also made significant contributions to the application of chaotic dynamics to communications, including the design and production of the first world-wide chaos-based communication MoDem chips. Some 30 high-performance mixed-signal chips were successfully designed by his team during the last 15 years in the framework of different R&D programs and contracts. These include three generation of vision chips for high-speed applications, analog front-ends for XDSL MoDems, ADCs for wireless communications, ADCs for automotive sensors, chaotic signals generators, complete MoDems for power-line communications, and more. Many of these chips are state-of-the-art in their respective fields, and some of them entered into mass production. In 2001, he was one of the cofounders of AnaFocus, a high-technology company focused on the design of mixed-signal circuits with emphasis on CMOS smart imagers and bio-inspired vision systems on chip. He has been heading Anafocus, Seville, Spain, since 2004.

Prof. Rodríguez-Vázquez has authored and/or edited eight books; around 40 chapters in contributed books, including original tutorials on chaotic integrated circuits, design of data converters and design of chips for vision, and more than 400 articles in peer-review specialized publications. He has served as Editor, Associate Editor, or Guest Editor for many IEEE and non-IEEE journals, as chairman for many international conferences and is on the committees of some international journals and conferences. He has received a number of international awards for his research work (including the IEEE Guillemin-Cauer Best Paper Award) and was elected Fellow of the IEEE for his contributions to the design of chaos-based communication chips and neuro-fuzzy chips.